Step-by-step advancement of the charge density wave in the rf-synchronized modes and oscillations of the width of Shapiro steps with respect to the rf power applied

S. G. Zybtsev,[1] S. A. Nikonov,[1] V. Ya. Pokrovskii,[1,*] V. V. Pavlovskiy,[1] and D. Starešinić[2]
[1]*Kotel'nikov Institute of Radioengineering and Electronics of RAS, Mokhovaya 11-7, 125009 Moscow, Russia*
[2]*Institute of Physics, Bijenička cesta 46, HR-10000 Zagreb, Croatia*

(Received 1 November 2019; revised manuscript received 11 February 2020; accepted 24 February 2020; published 24 March 2020)

The sliding of the room-temperature charge density wave (CDW) in the monoclinic phase of NbS_3 under rf power is studied. The threshold field, E_t, and Shapiro steps' width, δE, show aperiodic Bessel-type oscillations as a function of rf voltage. Here we demonstrate experimentally that, if presented as a function of CDW path length in each half period of the rf voltage, E_t and δE show *periodic* oscillations, the period being equal to the CDW wavelength. The result is found to be universal for different compounds and gives clear understanding of the synchronization effects in terms of forced oscillations of a particle in a periodic potential.

DOI: 10.1103/PhysRevB.101.115425

I. INTRODUCTION

Sliding of the charge density waves (CDW) in quasi-one-dimensional conductors [1,2] is always opposed by some kind of pinning. In all the cases the pinning force is periodic in the CDW displacement, with the period typically equal to λ, the CDW wavelength. Therefore the CDW sliding can be characterized with the fundamental (or "washboard") frequency f_f proportional to the CDW velocity: during the time $1/f_f$ the CDW travels by one wavelength, λ, or, in terms of phase, gains phase $\delta\varphi = 2\pi$.

rf interference is one of the characteristic and fascinating features of the CDWs in quasi-one-dimensional conductors [1–3]. ac voltage at a frequency, f, varying from the kHz to GHz region, if applied to the sample, can result in the synchronization of CDW sliding. This happens when the fundamental frequency, f_f, or one of its harmonics or subharmonics, coincides with f. Then the ac field begins to "dictate" the velocity of the CDW sliding preventing its change. As a result, ranges of electric field, E, appear on the I-V curves, over which the nonlinear current, I_{nl}, i.e., the current provided by the CDW, is constant or nearly constant. These ranges, δE_i (or δV_i in voltage units) are usually referred to as Shapiro steps (ShSs), where i is the number of the step. The ShSs can be better seen in the "differential I-V curves", i.e., in the dependences of the differential conductivity, $\sigma_d \equiv dI/dV$, on dc voltage V_{dc}. In this presentation the ShSs appear as dips on the $\sigma_d(V_{dc})$ curves. In case of complete CDW synchronization, or "mode locking," σ_d drops down to the level of quasiparticle conductivity, $\sigma_d(0)$.

The ShSs were primarily observed in Josephson junctions (JJs) [4,5], later—in the vortex flux-flow mode [6]. The phenomenon points out a similarity of physics of CDW and superconductivity. In both physical systems the ShSs show oscillations of widths as a function of rf voltage rms value, V_{rf} [3,5,7–10]. Similarly, oscillations of the threshold field, E_t (or voltage, V_t) can be observed in CDW systems [8–10], akin to the oscillations of the critical current of the JJs. The oscillations in superconducting systems are well described by the aperiodic Bessel function of the rf voltage [5].

The similarity of the effects in CDW with superconductors at first inspired the description of CDW dynamics in terms of Zener tunneling across a gap [11,12] later attributed to the collective pinning [8,13]. The shapes of the I-V curves in CDW samples appeared quite similar with those of JJs (with I and V interchanged), and the description of the oscillations with the Bessel function appeared more or less successful. However, further studies of the CDW dynamics in different compounds, and in the samples of different dimensions, purity, and defect structure showed that the physics of CDW depinning and dynamics can be rather rich [14]. A number of different models, such as dynamic phase transition [15], coherent creep [16], and phase-slippage controlled depinning [17] have been suggested, each being a success in a particular case. The tunneling model associated with the name of John Bardeen was rejected, mainly because of the unreasonably small values of the tunneling barrier [14]. This resume of the CDW studies is that the physics of CDW is much more diverse than that of superconductors.

The understanding of the oscillations of E_t and δE_i vs rf voltage has evolved together with the understanding of the CDW dynamics. In the publications following Ref. [8] the tunneling model was not considered as the central one [18], while the oscillations appeared to be only roughly described by the Bessel function [19]. Evidently, for each model of CDW dynamics one will get an individual description of the oscillations as a function of V_{rf}.

The goal of the present work was to find a general treatment of the ShSs, which could explain the oscillations of their magnitude, and would be independent of the mechanism of the CDW transport. The starting idea was that the conditions of synchronization must be uniquely defined by *the time-dependent travel of the CDW on the length scale of the washboard potential,* and that this travel *can be directly found from the experiment.*

*pok@cplire.ru

For the present studies we chose the monoclinic phase of NbS_3 (NbS_3-II). This typical CDW conductor is at the same time unique showing three CDW transitions, one of which is above and another—well above the room temperature, with $T_{P1} = 360$ K and $T_{P0} \approx 460$ K, correspondingly. The third CDW forms at $T_{P2} = 150$ K. All the three CDWs, CDW-1, CDW-0, and CDW-2 can slide in electric field. The transport of CDW-1 shows extremely high coherence and the highest frequencies of the synchronization, up to nearly 20 GHz [10]. Oscillations of V_t and δV_i vs rf voltage were recently reported for CDW-1 [10]. We chose NbS_3-II for the present studies not only because of the high coherence of CDW-1 and of the convenience of studies at room temperature, but also because of its fast response to the changing electric field. The latter will be important for the processing of the experimental results.

In this paper we report multiple oscillations of E_t and δE_i as a function of rf voltage at frequencies $f = 20$–400 MHz and show experimentally that they are periodic in CDW displacement during each half period of the rf field. In particular, we show that the first minimum of E_t corresponds to rf voltage inducing CDW displacement by λ forward and back, the second minimum by 2λ, etc. As for ShSs, δE_1 shows the first minimum when the CDW advances by 2λ during the first half period and returns back by λ during the other half period, the second when it advances by 3λ and returns by 2λ, etc. The oscillations appear periodic in the half difference of the CDW displacements during the first and second half periods of the rf voltage, the period being equal to λ. The even harmonics (including E_t, the "zeroth" harmonic) oscillate in antiphase with the odd ones.

These results are repeated on two different CDW compounds, $NbSe_3$ and TaS_3, and find an evident physical interpretation in terms of oscillations in the washboard potential. For example, the first minimum of E_t is observed, when the ac voltage swings the CDW up to the edges of the well of the potential.

II. APPROACH AND BASIC ASSUMPTIONS

The relaxation rates (inverse relaxation times) for the CDWs are known to lie in the GHz range and above (see Ref. [20] for orthorhombic TaS_3 (o-TaS_3) and $NbSe_3$). Although the pinning frequency was not measured for CDWs in NbS_3-II, the frequencies up to 20 GHz of ShSs [10] argue that CDW-1 shows rather small relaxation times. Therefore, we consider CDW-1 (below we name it just "CDW") as a massless overdamped object. As the frequencies of rf voltage, within 400 MHz in our experiments, are well below the inverse relaxation times characterizing the dynamics of CDW-1, CDW responds instantaneously to the external voltage. This allows analyses of the CDW travel under mixed ac-dc field basing on the shape of the stationary *I-V* curves, obtained *without* rf field. In particular, given time-dependent voltage, $V(t)$, and the $I_{nl}(V)$ curve one gets the values of CDW current at each point of time. Knowing the ratio I_{nl}/f_f, namely the ratio of nonlinear current, I_1, at the first ShS to the rf frequency, one can rescale the instantaneous value of I_{nl} into the corresponding fundamental frequency.

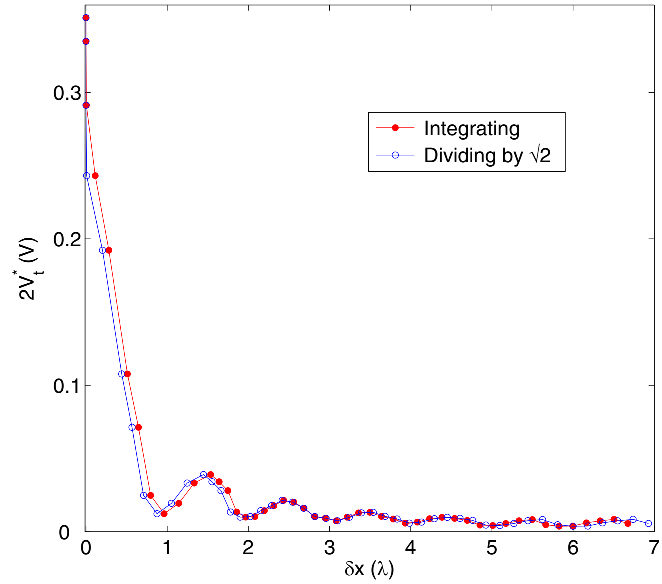

FIG. 1. Values of $2V_t^*$ vs $\delta x \equiv (\delta x_1 – \delta x_2)/2$ under sine-wave rf voltage applied. Here $\delta x = \delta x_1 = -\delta x_2$ and is found two ways: integrating the CDW current under time-dependent voltage and calculating the travel under square-wave voltage with the same rms value. Sample No. 1, 20 μm $\times$ 1.4 $\times$ 10^{-2} μm^2.

It is also implied that the CDW velocity is only slightly modulated by the washboard potential [21]. The latter assumption looks reasonable, at least, for CDW displacements by integer number of wavelengths, when the periodic velocity variation averages out.

Below, we start the analysis of the CDW dynamics under the effect of square-wave rf voltage, for which the estimates of the CDW travels are most simple. Under dc voltage, V_{dc}, mixed with rf voltage of amplitude V_{rf} (coinciding with its rms value) the CDW current will have the form of rectangular wave switching between two levels: $I_{nl}|_{V=V\mathrm{dc}+V\mathrm{rf}}$ and $I_{nl}|_{V=V\mathrm{dc}-V\mathrm{rf}}$. Then, knowing f_f at each half period of the rf voltage, $f_f|_{V=V\mathrm{dc}+V\mathrm{rf}}$ and $f_f|_{V=V\mathrm{dc}-V\mathrm{rf}}$, we can find the corresponding displacements of the CDW in a given time interval. In particular, the advancement of the CDW during each half period of the rf voltage, $t = 1/2f$, in units of λ equals $\delta x_1 = f_f|_{V=V\mathrm{dc}+V\mathrm{rf}}/2f$ and $\delta x_2 = f_f|_{V=V\mathrm{dc}-V\mathrm{rf}}/2f$ [23]. The equivalent form is $\delta x_{1,2} = I_{nl}|_{V=V\mathrm{dc}\pm V\mathrm{rf}}/2I_1$. V_{dc} is taken in the center of a ShS.

For calculating the CDW travel under the sine-form rf voltage, its value was divided by $\sqrt{2}$. Alternatively, the CDW travel was calculated integrating the CDW current over the changing in time sine-form voltage. Both approaches gave similar results with only a slight difference at small voltages, $V_{rf} \sim V_t$ (see Fig. 1).

III. EXPERIMENT

The most coherent CDW sliding can be observed in the high-Ohmic samples [10]. Therefore, we selected high-quality NbS_3-II samples from the high-Ohmic "subphase" with typical cross-sectional area 10^{-2} μm^2. A pair of gold contacts separated by 20–50 μm was deposited on each sample with laser ablation technique. The $\sigma_d(V_{dc})$ curves were measured

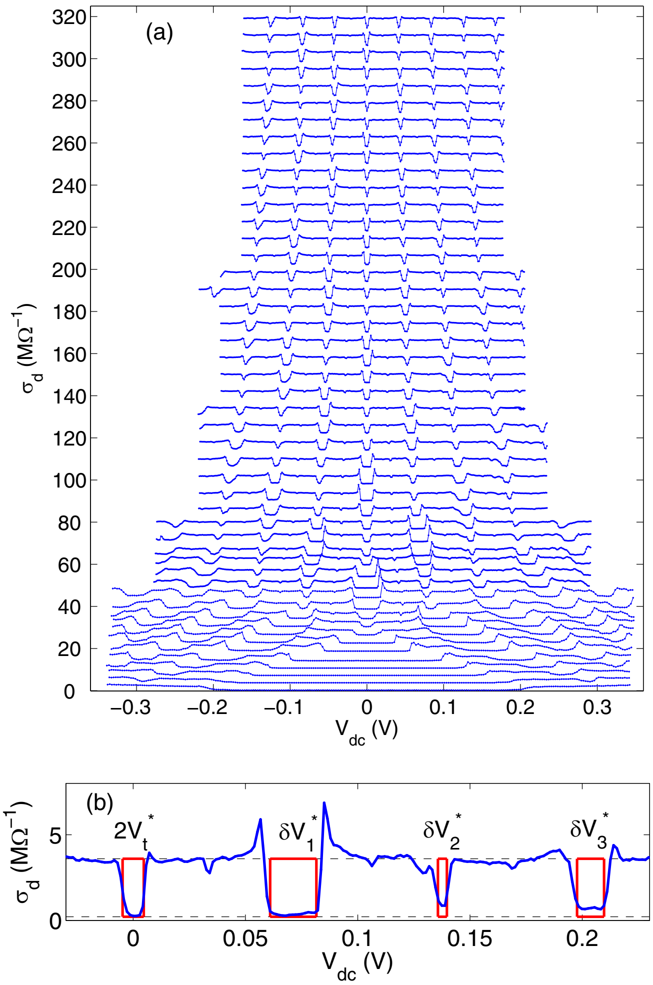

FIG. 2. (a) A set of σ_d vs V_{dc} curves under sine-wave rf irradiation with V_{rf} increasing in equal steps from 0 to 0.9 V (upper curve), for Sample No. 1. All the curves, except for the lower one, are shifted upwards in increments of $6.8\,\mathrm{M}\,\Omega^{-1}$. $f = 75\,\mathrm{MHz}$. (b) A fragment of one of the σ_d vs V_{dc} curves (at $V_{rf} = 290\,\mathrm{mV}$). The rectangles have the same areas as the correspondent dips. Their widths give the values of $V_t{}^*$ and $\delta V^*{}_i$. The broken lines show the levels of $\sigma_d(0)$ and $\sigma_d(\infty)$ (see text).

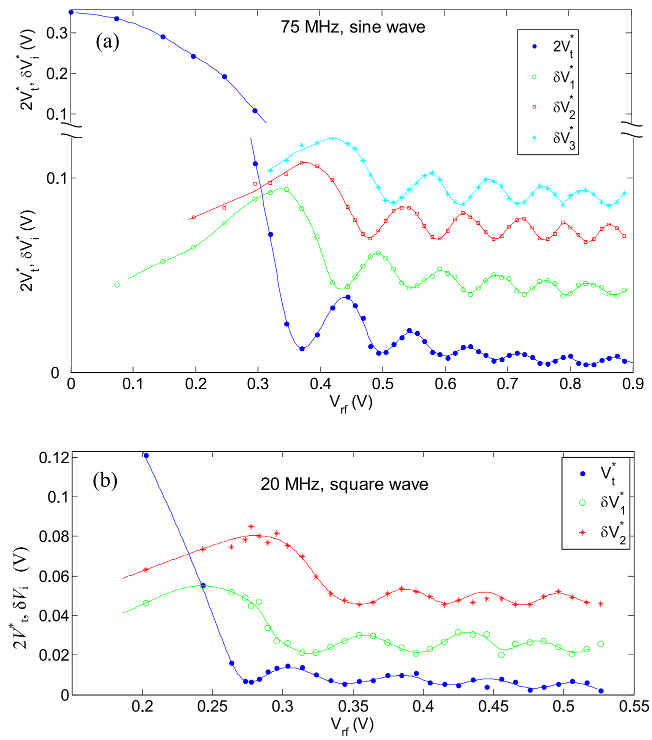

FIG. 3. (a). Values of $2V_t{}^*$ and $\delta V^*{}_i$ of the first three steps ($i = 1$–3) vs rf voltage for sample No 1. $f = 75\,\mathrm{MHz}$ (see Fig. 2). (b) Similar dependences ($i = 1$–2) under square-wave ac voltage at $f = 20\,\mathrm{MHz}$ for sample No. 2. ($35\,\mu\mathrm{m} \times 1.05 \times 10^{-2}\,\mu\mathrm{m}^2$). $2V_t{}^* \approx 2 \times 0.17\,\mathrm{V}$ at $V_{rf} = 0$. The solid lines are guides for the eye. The $\delta V^*{}_i(V_{rf})$ curves are shifted upwards.

at room temperature with the conventional lock-in technique. The rf voltage was applied to the NbS_3-II samples through a coupling capacitor. At $f = 20$–$80\,\mathrm{MHz}$ the commercial generator AKTAKOM AWG-4082 (Russia) was used. For f below 40 MHz it could be switched into the square-wave mode. For generating voltage at f up to 400 MHz we used the Γ4-144 generator (made in USSR). Special probes, the units of the high-frequency oscilloscopes LeCroy HDO6104 and Tektronix TDS3054C, were applied for calibration of the rf voltage directly at the samples' terminals at $f < 100$ MHz to the accuracy of about 5%.

IV. RESULTS

Figure 2(a) presents a set of $\sigma_d(V_{dc})$ curves measured for the sample No. 1 under sine-wave rf irradiation of different amplitudes. All the curves measured under nonzero rf voltage show distinct suppression of the threshold field and ShSs as dips of σ_d at $V > V_t$. In this presentation the vertical shift of the curves is proportional to the rf voltage, and one can notice nonsinusoidal oscillations of V_t and of the width of ShSs vs V_{rf}.

Before presenting the oscillations of the threshold voltage and Shapiro steps, it is necessary to define how to measure their magnitudes. A change of V_{rf} modifies both the width and the amplitude of the ShSs. Below, we rescale the dips to complete synchronization, i.e., replace each of them by a rectangle with upper and lower sides at $\sigma_d(\infty)$ and $\sigma_d(0)$, respectively, and having the same area as the original dip [Fig. 2(b)]. Here, $\sigma_d(\infty)$ is the saturation value of conductivity above V_t, which is well defined for the highly coherent CDW (Fig. 2). The width of such a rectangle, $\delta V^*{}_i$, gives the magnitude of the ShS. (Integrating the peaks' area in *dV/dI* vs I_{dc} axes [3] gives approximately the same result).

Similarly, the decrease of V_t is accompanied by a change of the shape of the I-V curve around $V_{dc} = 0$. Particularly, with the increase of V_{rf} the V_t value at first falls down to zero, and then the dip of the $\sigma_d(V_{dc})$ around $V_{dc} = 0$ begins to decrease. By analogy with ShSs, we rescaled each $\sigma_d(V_{dc})$ curve into a rectangular $2V_t{}^*$ wide and $\sigma_d(\infty)$-$\sigma_d(0)$ high [Fig. 2(b)].

Figure 3(a) shows the values of $2V_t{}^*$ and $\delta V^*{}_i$ for $i =$ 1–3 as functions of rf amplitude for the sample presented in Fig. 2. Like in Refs. [8] and [10] they show aperiodic oscillations, which tend to become periodic at large values of V_{rf}. Figure 3(b) shows similar curves for another sample under square-wave ac voltage of 20-MHz frequency. For the low-frequency rf signal the ShSs are located very dense along the $V_{\rm dc}$ axis, and the oscillations of $V_{\rm t}^*$ and $\delta V^*_{\rm i}$ are not so pronounced. However, as we mentioned above, the travel of CDW under square-wave voltage can be more easily estimated. Therefore, we begin the processing of our results with the data presented in Fig. 3(b).

V. PROCESSING OF EXPERIMENTAL RESULTS

The $I_{\rm nl}(V_{\rm dc})$ dependence at $V_{\rm rf}=0$ for the sample No. 2 is shown in the inset to Fig. 4(a). The ShSs give the ratio $I_{\rm nl}/f_{\rm f}=2.37$ nA/MHz for this sample, and thus the $I_{\rm nl}(V_{\rm dc})$ curve can be rescaled into the $f_{\rm f}(V_{\rm dc})$ dependence.

Figure 4(a) shows the values of $V_{\rm t}^*$ and $\delta V^*_{\rm i}$ vs CDW displacements in units of λ for sample No. 2. Here the x axis shows the half difference between the CDW displacements within the two half periods, $\delta x \equiv [f_{\rm f}|_{V=V{\rm dc}+V{\rm rf}}/2f - f_{\rm f}|_{V=V{\rm dc}-V{\rm rf}}/2f]/2 \equiv (\delta x_1 - \delta x_2)/2$. In a general sense, δx can be considered as the measure of the effect of rf voltage on the CDW travel: in the limit of $V_{\rm rf}\to 0$, $\delta x\to 0$ as well. In other words, δx indicates the CDW travel at each half period in the frame moving with the CDW average velocity. With the exception of the smallest $V_{\rm rf}$, the δx_1 and δx_2 values indicate CDW displacements in opposite directions. Thus, $2\delta x = |\delta x_1| + |\delta x_2|$ and can be also considered the total travel of the CDW during one period of the rf voltage. In the particular case of $V_{\rm dc}=0$ (resting frame, zeroth ShS) δx gives the CDW displacements at each half period of rf voltage, which are equal and opposite in signs: $\delta x_1 = -\delta x_2$.

In Fig. 4(a) the results are better visible for the oscillations of $V_{\rm t}^*$. One can see that the first minimum of $V_{\rm t}^*$ corresponds to $\delta x = 1$. The second $V_{\rm t}^*$ minimum is around $\delta x = 2$, the third around $\delta x = 3$, although these minima are worse defined.

More clear results can be found for the case of higher-frequency rf voltage of sine-wave form applied to the whisker [Fig. 3(a)]. Here, the CDW travel was calculated by replacing the sine-wave signal by a rectangular one with amplitude divided by $\sqrt{2}$ (Fig. 1).

In the synchronized modes the sum $\delta x_1 + \delta x_2$ must be equal to λ for the first ShS, 2λ for the second ShS, etc. [24]. The check of this condition is presented in Appendix A, where the calculated values of δx_1, δx_2, and $\delta x_1 + \delta x_2$ at different ShSs are shown as a function of rf voltage (see Fig. 9). Thus, this figure displays a "checksum" for the determination of the CDW travel and gives an estimate of a possible discrepancy of $\delta x_{1,2}$ with the actual values.

The oscillations appear periodic plotted either as a function of CDW displacement during each half period of rf voltage, i.e., δx_1 or δx_2 [Fig. 4(b)], or of δx [Fig. 4(c)]. In both presentations the period of oscillations of $V_{\rm t}^*$ and $\delta V^*_{\rm i}$ is the same and close to λ (Fig. 5). The first minimum of $V_{\rm t}^*$ is achieved when the rf voltage swings the CDW by λ, the second by 2λ, etc. [see also Fig. 4(a)]. In the δx units δV^*_1 oscillates in antiphase to $V_{\rm t}^*$ [Fig. 4(b)]. In general, for even i the ShSs oscillate in phase with $V_{\rm t}^*$, for odd i in antiphase. Thus, $V_{\rm t}^*$ value behaves as the zeroth harmonic, demonstrating again that the part of I-V curve between $-V_{\rm t}$ and $+V_{\rm t}$ could be treated as the zeroth ShS.

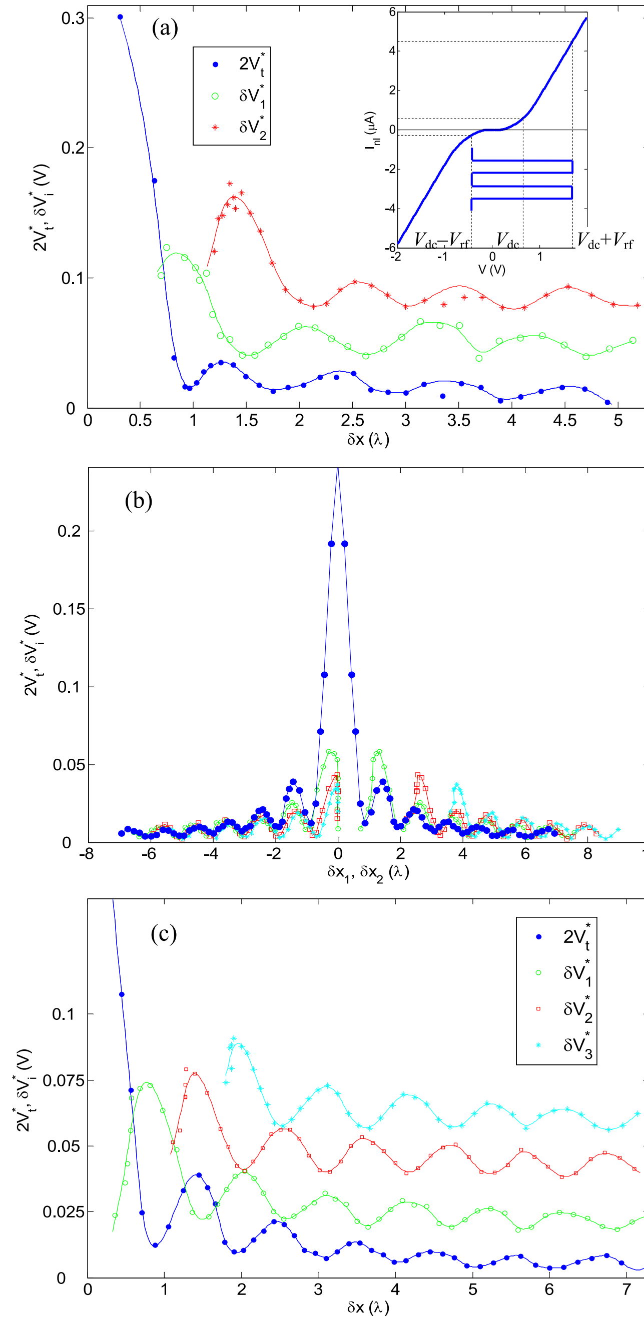

FIG. 4. (a) $2V_{\rm t}^*$ and $\delta V^*_{\rm i}$ ($i = 1$–2) for sample No. 2 vs δx. Rectangular rf voltage is applied [see Fig. 3(b)]. The $\delta V^*_{\rm i}(V_{\rm rf})$ curves are shifted upwards. Inset: $I_{\rm nl}$ vs $V_{\rm dc}$ dependence without irradiation. The dashed lines illustrate the definition of $I_{\rm nl}$ (and $f_{\rm f}$) for the calculation of CDW travels in each of the half periods of the rectangular voltage. (b) $2V_{\rm t}^*$ and $\delta V^*_{\rm i}$ ($i = 1$–3) vs δx_1 (the positive values) and δx_2 (the negative or 0 values) for sample No. 1 exposed to sine-wave rf voltage [see Fig. 3(a)]. The same vs δx is shown in panel (c). The $\delta V^*_{\rm i}(V_{\rm rf})$ curves are shifted upwards. The solid lines are guides for the eye.

We also observed oscillations under rf voltage with 400-MHz frequency. Although we did not calibrate $V_{\rm rf}$ at the sample terminals in this case, with a single fitting parameter, i.e., the coefficient of the rf voltage attenuation, we obtained

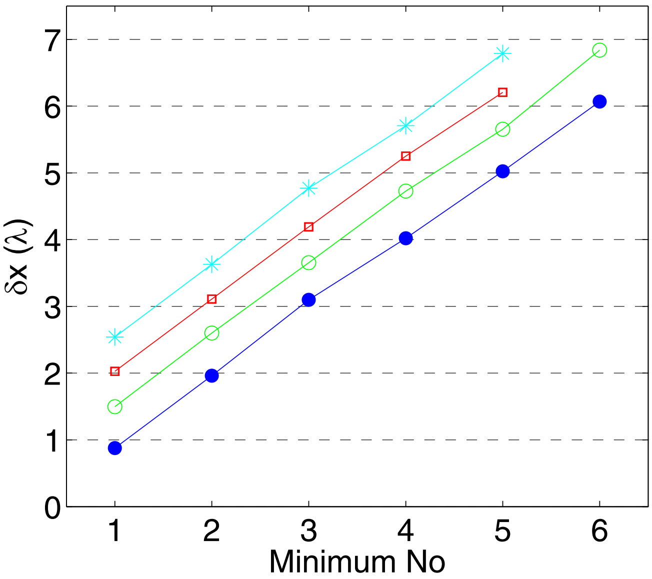

FIG. 5. The δx values at the minima of $V_t{}^*$ (•), $\delta V^*{}_1$ (○), $\delta V^*{}_2$ (□), and $\delta V^*{}_3$ (∗) vs the minimum number. Sample no 1.

periodic oscillations of $V_t{}^*$ and $\delta V^*{}_i$, similar with those in Figs. 4(b) and 4(c).

The higher is f, the longer is the period of $V_t{}^*$ oscillations in units of V_{rf}. In fact, higher voltage is needed for CDW to pass the same way, λ, in the shorter time, $1/2f$. This clarifies the statement of Ref. [8] that the period of the oscillations is roughly proportional to the ac frequency.

To check if the periodicity of the oscillations as a function of δx is universal, we tested the procedure on two different CDW compounds: $NbSe_3$, where such oscillations have been studied previously in detail, and o-TaS_3, for which the oscillations have not yet been reported. On both compounds we observed oscillations of E_t and δE_1. The experiment and the results of its processing are presented in Appendix B. We found that the maxima and minima of the zeroth and the first ShSs are placed at the same values of the δx, as for NbS_3 [Figs. 4(a) and 4(c)] (see also Ref. [25]). Thus, the result of the rescaling of the oscillations is universal for different compounds.

VI. DISCUSSION

The physical sense of $V_t{}^*$ oscillations is most transparent. In terms of the washboard potential, under small V_{rf} in the stationary regime the CDW is oscillating around the potential minimum [Fig. 6(a)]. The higher is V_{rf}, the larger is the amplitude. When the swing of the oscillations is approaching λ, i.e., the CDW is oscillating by nearly $\pm\lambda/2$ around the minimum, it nearly reaches the highest energy at the return points, as shown in Fig. 6(a). Any dc voltage would throw the CDW over the corresponding energy maximum into the neighboring valley. Although after sign reversal of the rf voltage the CDW will return to the "home" valley, the next rf wave will cast it further into the new valley, etc. Thus, due the positive feedback, the CDW will begin to travel gradually, giving rise to a charge transfer. Therefore, at this V_{rf} value $V_t{}^*$ will show a minimum (in the ideal case—zero), in agreement

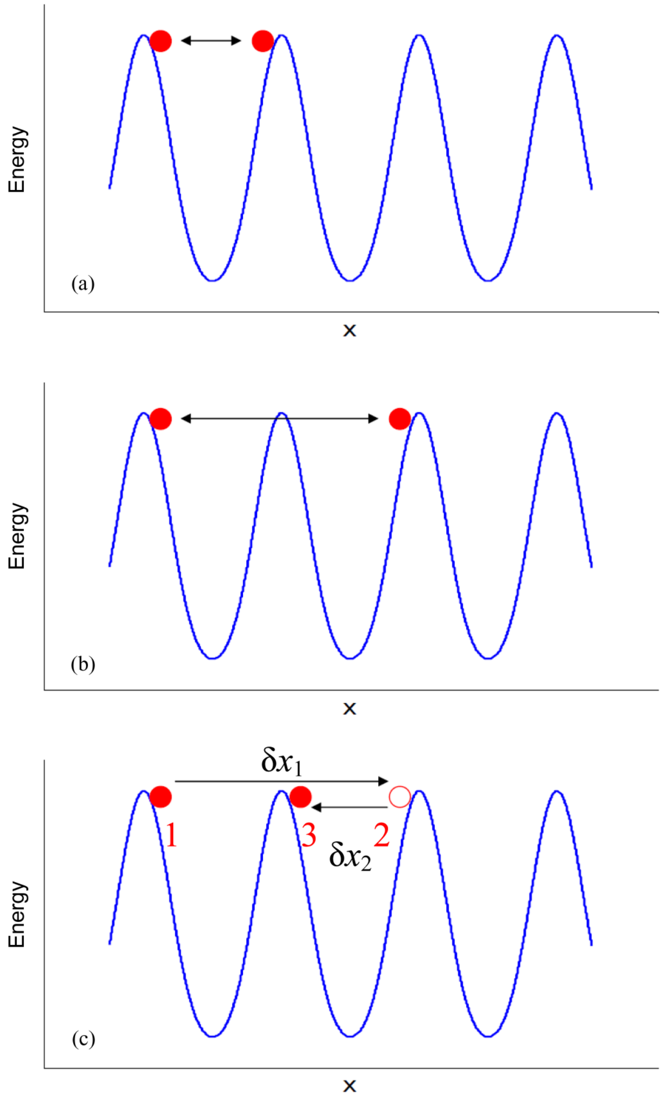

FIG. 6. Illustrations of the effects of rf voltage on V_t (a), (b) and δV_1.(c). (a) corresponds to the first minimum of V_t, (b) to the second, and (c) corresponds to the first minimum of δV_1.

with the experiment (Fig. 4). A similar consideration can be repeated for rf voltage inducing CDW oscillations with sweep of 2λ [Fig. 6(b)], 3λ, etc. It is remarkable and contrary to intuition that the central point of the oscillations by $\pm\lambda$ (and somewhat less) is positioned at a potential maximum. However, calculations for a JJ (see below) justify that this can occur.

Note that the minima of $V_t{}^*$ correspond to CDW travels by integer numbers of λ, the case for which the determination of δx is most exact. The minima of $\delta V^*{}_i$ also match integer δx_1 and δx_2 values. For example, the minima of $\delta V^*{}_1$ correspond to δx_1 and δx_2 equal to 2 and -1, 3 and -2, 4 and -3, etc. [Fig. 4(b)]. For $\delta V^*{}_2$ minima δx_1 and δx_2 are close to 2 and 0, 3 and -1, 4 and -2, etc., respectively [Fig. 4(b)].

The similarity of $V_t{}^*$ and $\delta V^*{}_i$ variations suggests considering the mode locking as forced oscillations of the CDW in the washboard potential as well. By analogy, at the minima of $\delta V^*{}_i$ the return points appear near the potential maxima. How-

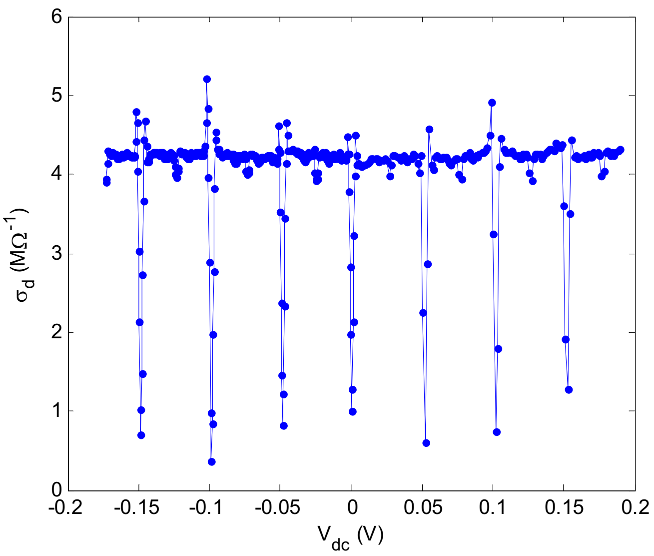

FIG. 7. Example of σ_d vs V_{dc} curve under irradiation. Only the $V_{dc} = 0$ tick allows distinguishing the zeroth ShS from others. Sample No. 3, 21 μm × 1.3 × 10^{-2} μm^2. $f = 80$ MHz, $V_{rf} = 840$ mV.

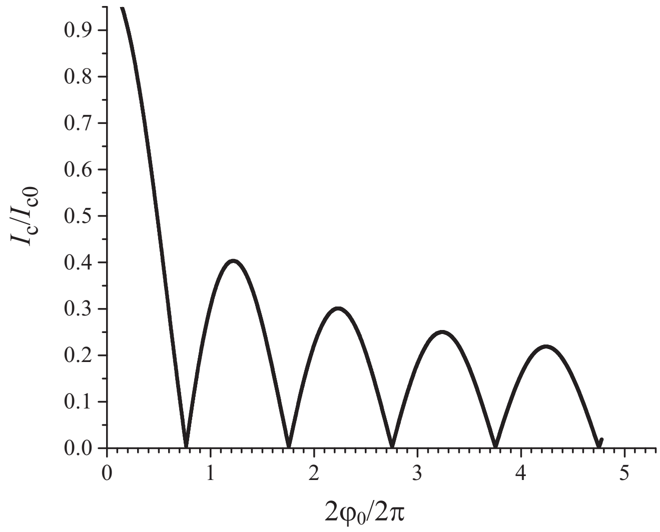

FIG. 8. Normalized Josephson critical current I_c/I_{c0} as a function of the phase sweep $2\varphi_0$ normalized by 2π. I_{c0} is critical current in the absence of external radiation. $f/f_c = 20$ ($f_c = eV_c/\pi\hbar$).

ever, for the case of ShSs the oscillations appear asymmetric in the forward and back paths.

Figure 6(c) illustrates δx_1 and δx_2 for the case when the first ShS approaches its first minimum: the CDW jumps forward by $\delta x_1 = 2$, and then returns back by $\delta x_2 = -1$ ($\delta x = 1.5$). Any change of V_{dc} will break the synchronization condition. The effect of V_{dc} variation is similar with that of small V_{dc} on V_t^* at its first minimum [Fig. 6(a)], which we considered above. For lower or larger values of V_{rf} (and δx) the CDW oscillates between points below the potential maxima, and the oscillation becomes stable upon the variations of V_{dc}. Thus, the width of the ShS grows with deviation of δx from 1.5.

The amplitude of the ShSs as a functions of back-forward jumps in the washboard potential has been discussed also in the theoretical paper [19]. The similar considerations of V_t^* and δV^*_i variation further clarify the common origin of the effects, which can be treated as resonance phenomena (see also Refs. [26,27]). In some experiments it was easy to mix-up the ShSs and the point $V_{dc} = 0$ on the $\sigma_d(V_{dc})$ curves. Figure 7 shows such an example.

According to Fig. 4, the maxima of V_t^* (except for the trivial case of $V_{rf} = 0$) or δV^*_i correspond to half integer $\delta x_{1,2}$. In this case the CDW oscillates approximately between the middles of the slopes of the washboard potential. The large slopes at the return points give rise to the high negative feedback on a variation of V_{dc}. This explains the stability of the ShSs. However, this conclusion is not as intuitively evident as for the minima of the ShSs. A particular model is needed for relating the maxima with δx. Here we are discussing only the qualitative consequences of our experiment, so we will not consider the ShSs maxima in detail. In addition, the calculation of the fractional $\delta x_{1,2}$ values could be not so exact because of the λ-periodic modulation of the CDW velocity.

We are making the only exception for the first maximum of the first ShS. It is achieved at δx a little bit below 1 [Figs. 4(b) and 4(c)]. One can see [Fig. 4(b)] that the ShS is noticeable only for $\delta x_2 \leqslant 0$. No synchronization is observed when the CDW is moving forward during both half periods of V_{rf} ($\delta x_{1,2} > 0$). The width of the ShS grows while $\delta x_2 = 0$, until the CDW begins moving back during the second half period. During this rest the CDW can restore its coherence: if some domains have fallen behind or passed ahead of the main stream during the first half period, they can relax during the second one down to the energy minimum and join the major CDW phase. This result corroborates with the conclusion of Ref. [28], where rectangular voltage has been applied to the samples as well. The authors noticed that for perfect mode locking the CDW must be at rest during some time interval, i.e., $V(t)$ should enter the range $|V| < V_t$ for some time. A similar explanation of the first maximum of the first ShS was suggested in Ref. [8].

Finally, we must note that a similar approach can be applied to JJs. The well-known analogy of CDW sliding and the Josephson effect [29] is based on the similarity of the CDW displacement equation and evolution equation of condensate phase φ in the resistively shunted junction (RSJ) model of JJ (see Appendix C for more detail). External rf electromagnetic radiation forces phase oscillations with an amplitude φ_0. The phase sweep in units of 2π, $2\varphi_0/2\pi$, is the analog of a CDW displacement δx under rf voltage at $V_{dc} = 0$. The resulting I_c vs $2\varphi_0/2\pi$ dependence is shown in Fig. 8. The oscillations appear periodic with the period equal to 1, which coincides with that of V_t oscillations (Fig. 4).

It is also important that the RSJ model provides the change of the central point of the oscillations with rf voltage. It confirms that when the phase sweep exceeds a certain value, namely, corresponding to the first zero of I_c, the oscillations become stabilized not around a minimum, but around a neighboring maximum of the periodic potential (see Fig. 12 in Appendix C), in concord with Fig. 6(b). At the next I_c zero the central point again switches to a minimum, etc.

VII. CONCLUSION

Multiple oscillations of the threshold field and Shapiro steps' width as a function of the amplitude of rf field have been reported for NbS_3-II, $NbSe_3$, and TaS_3. We have demonstrated a simple algorithm which transforms the Bessel-type oscillations into periodic ones. Namely, one should take the *I-V* curve of the sample without irradiation and get the $I_{nl}(V_{dc})$ dependence. Then, taking the time-dependent value of the ac+dc voltage across the sample, $V(t)$, one should integrate $I_{nl}[V(t)]$ with respect to time over each of the half periods of the rf voltage. Dividing the results by the ratio of I_{nl} to the fundamental frequency one will determine the corresponding CDW displacements in units of λ. Then, if plotted vs these displacements, or vs half difference of these displacements, E_t and δE will show periodic oscillations, the period being equal to λ.

In a sense, our studies have revealed the "proper" x axis for the oscillations, in which they appear periodic. As an illustration for this statement, one can make an example of the f dependence of the voltage or current of a ShS: the physical sense of the ShSs becomes clear when f is plotted vs the *nonlinear* current at the step, which can be treated as the proper x axis for scaling the fundamental frequency.

The result of the present studies is purely experimental and, at the same time, has a simple model-free physical sense. For example, the first minimum of E_t marks the rf voltage inducing oscillations by ±λ/2, whose self-stabilization around the minimum of the washboard potential is obvious for lower amplitudes. Accordingly, a small dc field will push the CDW in the next potential valley and, thus, depin it. The following variations of E_t with V_{rf} can be also described in terms of oscillations in the washboard potential, whose return points are self-stabilized at a certain level.

The variations of ShSs magnitudes can be treated in terms of forced oscillations of the CDW as well, although asymmetric in advancement forward and back in the periodic potential. In particular, the minima of ShSs correspond to oscillations of the CDW between return points coinciding with maxima of the potential.

Our experiment also clearly shows the common nature of E_t and δE variations with rf voltage.

ACKNOWLEDGMENTS

We are grateful to S. V. Zaitsev-Zotov for useful discussion. The support of RFBR (Grants No. 20-02-00827 and No. 18-02-00931) is acknowledged. The processing of the *I-V* curves was supported by the Russian Scientific Foundation (Grant No 17-12-01519). V.V.P. has analyzed the oscillations of ShSs in the Josephson junctions within the framework of the State task.

APPENDIX A: CHECK OF δx_i CALCULATIONS

Figure 9 shows δx_1, δx_2, and the calculated total displacement $\delta x_1 + \delta x_2$ for each ShS vs V_{rf}. At the ith ShS, according to the definition, the sum $\delta x_1 + \delta x_2$ must be equal to $i\lambda$, where $i = 0, 1, 2, 3, \ldots$ ($i = 0$ for V_t^*, the zeroth ShS). From Fig. 9 one can see that the resulting CDW displacements agree with the expectations for $i = 0$, 1, 2, 3 with the following reservations:

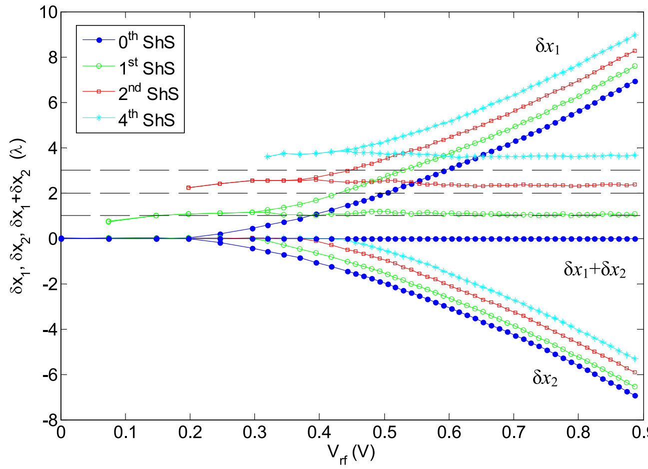

FIG. 9. δx_1, δx_2 and $\delta x_1 + \delta x_2$ vs rf voltage calculated at different ShSs for sample No. 1. The broken lines show the "control sums," i.e., the expected values of $\delta x_1 + \delta x_2$.

(1) One should take into account that although for $|V_{dc} - V_{rf}| < V_t$ according to the model the CDW is resting, actually it is moving within the potential well.

(2) For high values of i the calculated CDW displacement appears a little bit higher than $i\lambda$. The overestimate can be attributed to lag in CDW switching between the sliding states at $V_{dc} + V_{rf}$ and V_{dc}–V_{rf}, so that the actual CDW travel appears a little bit lower than the value calculated in the approximation of stationary sliding, i.e., instantaneous switching.

APPENDIX B: TEST OF THE δx_i VALUES FOR TaS_3 AND $NbSe_3$

See Figs. 10 and 11.

APPENDIX C: PHASE GAIN IN THE JOSEPHSON JUNCTIONS

The similarity of CDW and JJ can be achieved by substitution of electric field and current density in CDW case by Josephson current and voltage, correspondingly. Therefore E_t is replaced by Josephson critical current I_c, and CDW characteristic current $J_t = E_t/\rho_\infty$ can be defined similarly with Josephson characteristic voltage $V_c = I_c R_n$, where R_n is JJ normal-state resistivity and ρ_n is the CDW resistance in the high-voltage linear part of *I-V* curve.

JJ has a 2π phase-periodic energy:

$$E_j = \frac{\hbar I_c}{e}\sin^2\frac{\varphi}{2}, \qquad \text{(C1)}$$

where $\hbar$ is Planck's constant and e is electron charge [30]. External electromagnetic radiation of the amplitude V_{rf} forces ac current with the amplitude I_s through JJ and phase oscillations with the frequency f and the amplitude φ_0, which modify the observable dc critical current I_c. Unlike the case of CDW, the condensate phase φ cannot be measured, but, in return, the RSJ model perfectly describes the observable dynamics of JJ at temperatures near the critical one. I_c shows oscillating behavior with an increase of the rf power. It can be shown for the RSJ model that at the low-frequency limit ($f \ll$

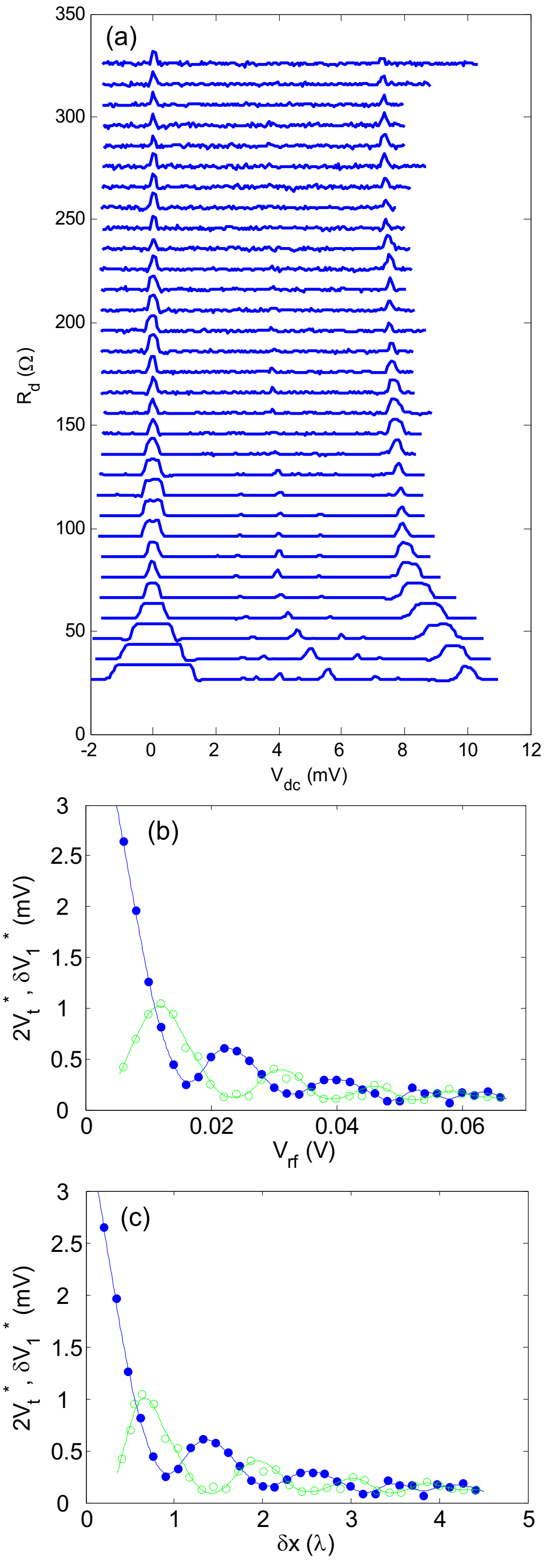

FIG. 10. NbSe$_3$ under 50-MHz irradiation. (a) A set of R_d vs V_{dc} curves under sine-wave rf irradiation with V_{rf} increasing in equal steps (from the lower to the upper curve). All the curves, except for the lower one, are shifted upwards. (b) Values of $2V_t^*$ and δV^*_1 vs V_{rf}. (c) Values of $2V_t^*$ and δV^*_1 vs δx. The studies were performed in the four-probe configuration. Distance between current probes, 716 μm; between potential probes, 83 μm; sample width, 6 μm; cross-sectional area, 3.5 μm^2. $T = 120$ K.

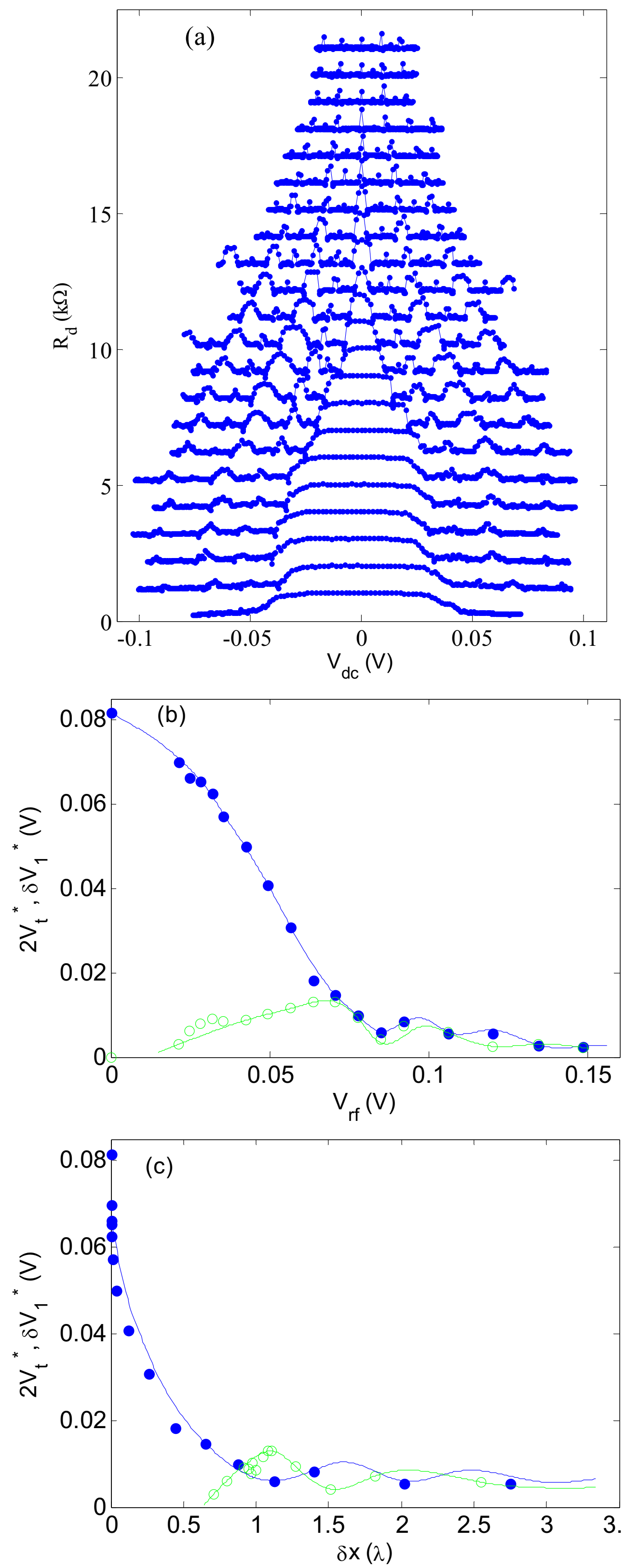

FIG. 11. TaS$_3$ under 10-MHz irradiation. (a) A set of R_d vs V_{dc} curves under sine-wave rf irradiation with V_{rf} increasing in equal steps (from the lower to the upper curve). All the curves, except for the lower one, are shifted upwards. (b) Values of $2V_t^*$ and δV^*_1 vs V_{rf}. (c) Values of $2V_t^*$ and δV^*_1 vs δx. Sample dimensions: 34 μm × 10^{-2} μm^2. $T = 120$ K.

f_c, where $f_c = eV_c/\pi\hbar)$ I_c is a periodic function of φ_0 with the period equal to π. Taking into account that the potential well width in (C1) is equal to 2π, this period corresponds to the extent of phase oscillations over one, two, etc. wells, similar to that in Fig 5.

At the high-frequency limit ($f \gg f_c$) an analytical expression for I_c can be obtained [30]:

$$\frac{I_c^*}{I_c} = J_0\left(\frac{I_s f_c}{I_c f}\right), \tag{C2}$$

where J_0 is the Bessel function. Using the relation $\varphi_0(I_s)$ calculated from the same model, one can show that the distance between $I_c(\varphi_0)$ zeros (or maxima) is multiple of π. While φ_0 is the amplitude of the phase oscillations, the phase sweep in units of 2π, $2\varphi_0/2\pi$, is equivalent to CDW displacement δx under rf voltage at $V_{dc} = 0$ (Fig. 4). The resulting I_c vs $2\varphi_0/2\pi$ dependence is shown in Fig. 8. One can see that the oscillations appear periodic with the period equal to 1, which coincides with that of V_t oscillations (Fig. 4).

For Fig. 8. the calculation was performed for relatively high frequency ($f/f_c = 20$). Although a direct estimate of f_c for the case of CDW is not obvious, for the experimental values of f the value of V_{rf} is well above V_t already at the first V_t minimum. Even for $f = 20$ MHz the correspondent value is $V_{rf} = 0.28$ V, while $V_t^* \approx 0.17$ V [Fig. 3(b)]. For $f = 75$ MHz the reserve is still higher [Fig. 3(a)]. This means that the effect of constant voltage $V_{dc} = V_{rf}$ on the CDW is stronger than the effect of the washboard potential, and we are close to the high-frequency limit. In this case an oscillating $V_t(V_{rf})$ dependence with decreasing amplitude is expected. It is only a Bessel-like dependence, because a true Bessel curve can be obtained only with a sinusoidal phase dependence of energy (C1), but nevertheless the $V_t(\delta x)$ dependences demonstrate equally spaced zeros similar to that in the ac Josephson effect (Fig. 8.).

The periodicity appears the same for different f values, but in the low-frequency limit the first zero of I_c corresponds to $2\varphi_0/2\pi = 1$, in contrast to $2\varphi_0/2\pi = y_1/\pi = 0.765$ in the high-frequency limit, where y_1 is the first Bessel function root value (Fig. 8). Our accuracy of rf voltage calibration does not allow to tell if δx is closer to 0.77 than to 1. One should keep in mind that although the f values in our experiment could be considered as high, the value 0.77 implies sinusoidal pinning potential.

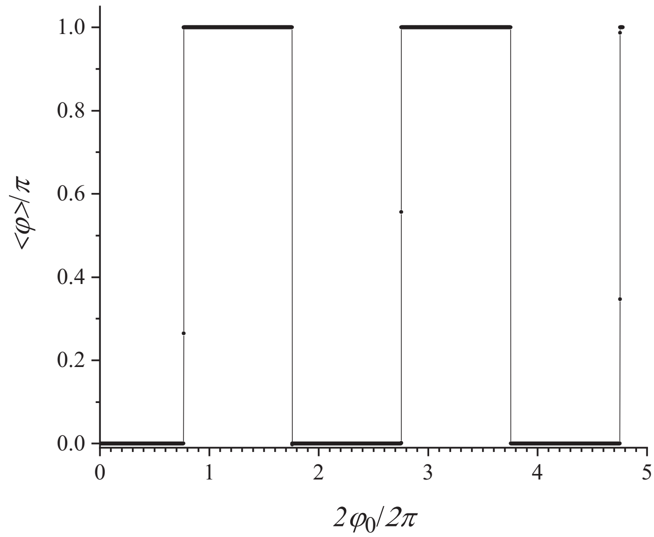

FIG. 12. Central point of the oscillations vs phase sweep $2\varphi_0$ normalized by 2π for $f/f_c = 20$.

It is also interesting that the RSJ model provides the change of the central point of the oscillations with rf voltage. It confirms that at a certain sweep of phase oscillations, namely, corresponding to the first zero of I_c, the oscillations become stabilized not around a minimum, but around a neighboring maximum of the periodic potential, Fig. 12, in concord with Fig. 6(b). At the next I_c zero the central point again switches to a minimum, etc.

[1] P. Monceau, in *Electronic Properties of Inorganic Quasi-One-Dimensional Conductors*, edited by P. Monceau (Reidel Publishing Company, Dordrecht, 1985), p. 2.

[2] P. Monceau, Adv. Phys. **61**, 325 (2012).

[3] S. Brown and A. Zettl, Charge density wave current oscillations and interference effects, in *Charge Density Waves in Solids*, edited by L. P. Gor'kov and G. Grüner (Elsevier North-Holland, Amsterdam, 1989), Vol. 25, p.223.

[4] S. Shapiro, Phys. Rev. Lett. **11**, 80 (1963).

[5] S. Shapiro, A. Janus, and S. Holly, Rev. Mod. Phys. **36**, 223 (1964).

[6] A. T. Fiory, Phys. Rev. Lett. **27**, 501 (1971).

[7] C. C. Grimes and S. Shapiro, Phys. Rev. **169**, 397 (1968).

[8] R. E. Thorne, W. G. Lyons, J. W. Lyding, J. R. Tucker, and J. Bardeen, Phys. Rev. B **35**, 6360 (1987).

[9] Yu. Latyshev, V. E. Minakova, and Yu. A. Rzhanov, JETP Lett. **46**, 37 (1987).

[10] S. G. Zybtsev, V. Y. Pokrovskii, V. F. Nasretdinova, S. V. Zaitsev-Zotov, V. V. Pavlovskiy, A. B. Odobesco, W. W. Pai, M.-W. Chu, Y. G. Lin, E. Zupanič *et al.*, Phys. Rev. B **95**, 035110 (2017).

[11] P. Monceau, N. P. Ong, A. M. Portis, A. Meerchaut, and J. Rouxel, Phys. Rev. Lett. **37**, 602 (1976).

[12] K. Maki, Phys. Rev. Lett. **39**, 46 (1977).

[13] J. Bardeen and J. Bardeen, Phys. Rev. Lett. **45**, 1978 (1980).

[14] R. E. Thorne, J. Phys. IV France **131**, 89 (2005).

[15] N. Ogawa, A. Shiraga, R. Kondo, S. Kagoshima, and K. Miyano, Phys. Rev. Lett. **87**, 256401 (2001).

[16] S. G. Lemay, K. O'Neill, C. Cicak, and R. E. Thorne, Phys. Rev. B **63**, 081102(R) (2001).

[17] O. C. Mantel, F. Chalin, C. Dekker, H. S. J. van der Zant, Yu. I. Latyshev, B. Pannetier, and P. Monceau, Phys. Rev. Lett. **84**, 538 (2000).

[18] R. E. Thorne, J. S. Hubacek, W. G. Lyons, J. W. Lyding, and J. R. Tucker, Phys. Rev. B **37**, 10055 (1988).
[19] B. Hu and J. Tekić, Phys. Rev. E **75**, 056608 (2007).
[20] S. Sridhar, D. Reagor, and G. Gruner, Phys. Rev. Lett. **55**, 1196 (1985).
[21] The periodic potential can be of any origin, including phase slippage [17], which can also show mode locking [22].
[22] D. Jelić, A. Bjeli, and I. Batistić, Phys. Rev. B **38**, 4045 (1988).
[23] For simplicity, we can take $V_{dc} > 0$; at the first half period $V = V_{dc} + V_{rf}$; at the second half period, $V = V_{dc} - V_{rf}$. Rescaling V into f_f we take negative f_f for negative V.
[24] This condition allows the solution of the inverse problem: Knowing the I-V curve without irradiation one can find the dc voltage of each ShS for given V_{rf}. (S. G. Zybtsev *et al.*, to be published).
[25] From the parameters presented in Table 1 of Ref. [8] it is possible to calculate I_{CDW} and f_f for $V_{dc} + V_{rf}$ and for $V_{dc} - V_{rf}$, and therefore also δx using the same approach as in the paper. The first minima of V_t at 2, 5, and 10 MHz correspond to $\delta x = 1.2$, 1, and 0.95, respectively.
[26] S. Bhattacharya, M. J. Higgins, and J. P. Stokes, Phys. Rev. B **38**, 7177 (1988).
[27] M. J. Higgins, A. A. Middleton, and S. Bhattacharya, Phys. Rev. Lett. **70**, 3784 (1993).
[28] S. E. Brown, G. Grüner, and L. Mihály, Solid State Commun. **57**, 165 (1986).
[29] M. Papoular, Phys. Lett. A **76**, 430 (1980).
[30] K. K. Likharev, *Dynamics of Josephson Junctions and Circuits* (Gordon and Breach, New York, 1986).